Published online June 21, 2004

Nucleic Acids Research, 2004, Vol. 32, No. 11 ***3325–3339***
DOI: 10.1093/nar/gkh654

Mcp7, a meiosis-specific coiled-coil protein of fission yeast, associates with Meu13 and is required for meiotic recombination

Takamune T. Saito, Takahiro Tougan, Takashi Kasama, Daisuke Okuzaki and Hiroshi Nojima*

Department of Molecular Genetics, Research Institute for Microbial Diseases, Osaka University, 3-1 Yamadaoka, Suita, Osaka 565-0871, Japan

Received April 22, 2004; Revised and Accepted May 26, 2004

ABSTRACT

We previously showed that Meu13 of *Schizosaccharomyces pombe* functions in homologous pairing and recombination at meiosis I. Here we show that a meiosis-specific gene encodes a coiled-coil protein that complexes with Meu13 during meiosis *in vivo*. This gene denoted as *mcp7*$^+$ (after *m*eiotic *c*oiled-coil *p*rotein) is an ortholog of Mnd1 of *Saccharomyces cerevisiae*. Mcp7 proteins are detected on meiotic chromatin. The phenotypes of *mcp7*Δ cells are similar to those of *meu13*Δ cells as they show reduced recombination rates and spore viability and produce spores with abnormal morphology. However, a delay in initiation of meiosis I chromosome segregation of *mcp7*Δ cells is not so conspicuous as *meu13*Δ cells, and no meiotic delay is observed in *mcp7*Δ*meu13*Δ cells. Mcp7 and Meu13 proteins depend on each other differently; Mcp7 becomes more stable in *meu13*Δ cells, whereas Meu13 becomes less stable in *mcp7*Δ cells. Genetic analysis shows that Mcp7 acts in the downstream of Dmc1, homologs of *Escherichia coli* RecA protein, for both recombination and subsequent sporulation. Taken together, we conclude that Mcp7 associates with Meu13 and together they play a key role in meiotic recombination.

INTRODUCTION

Meiosis is a special type of cell division that produces haploid gametes from diploid parental cells. In many eukaryotes, meiosis-specific events that are important for the generation of genetic diversity, such as synaptonemal complex (SC) formation, homologous pairing and recombination, occur at meiotic prophase I (1–3). Meiotic recombination is initiated by double-strand breaks (DSBs) in the genomic DNA that are catalyzed in *Saccharomyces cerevisiae* and *Schizosaccharomyces pombe* by the topoisomerase-like proteins Spo11 (4) and Rec12 (5–7), respectively. Mutants of *spo11* in *S.cerevisiae* and the *spo11* homologs in *Arabidopsis thaliana* and *Mus musculus* that are incapable of initiating homologous recombination show defects in homologous pairing and/or synapsis formation (8–10).

Since homologous recombination is critical for the generation of viable gametes, a mechanism in *S.cerevisiae* called the pachytene checkpoint is known to prevent meiotic progression at the pachytene stage if abnormal recombination and/or chromosome synapsis occur (11). In contrast, a mechanism in *S.pombe* called the meiotic recombination checkpoint delays initiation of meiosis I chromosome segregation but does not arrest at meiotic prophase I (12). Notably, this delay is tightly linked to the prolonged inactivation of Cdc2 due to the phosphorylation of its tyrosine 15 residues, an event that is dependent on the checkpoint *rad*$^+$ genes (12). The proteins involved in the DNA damage checkpoint also participate in the pachytene checkpoint in *S.cerevisiae* and the event depends on the formation and processing of DSBs (13). This mechanism also seems to be conserved in mammals since the Atm, Atr, Rad1 and Chk1 proteins that are involved in the damage checkpoint localize to the meiotic chromosomal cores and are thought to play important roles in recombination and meiotic arrest (14).

In *S.cerevisiae*, Hop2 plays a crucial role in the proper alignment of homologous chromosomes during meiotic prophase and functions in the same pathway with Rad51 and Dmc1, two homologs of *E.coli* RecA (15,16). *Hop2* knockout mice display similar phenotypes to *hop2* mutant of *S.cerevisiae* such that spermatocytes arrest at the stage of pachytene-like chromosome condensation and the meiotic DSBs fail to be repaired (17). Thus, the Hop2 functions seem to be conserved in mammals. It should be remembered, however, that a Hop2 ortholog has not been found in *Drosophila melanogaster* and *Caenorhabditis elegans* and that recombination itself is not required for either homologous pairing or synapsis in mutants of the *spo11* homologues in these organisms (18,19). Thus, the mechanisms regulating meiotic pairing and recombination in these species seem to differ from those in many other organisms.

Schizosaccharomyces pombe is a useful model organism for the study of meiotic recombination, checkpoint and chromosome pairing because it lacks SC formation and harbors only three chromosomes. This makes it possible to study the

*To whom correspondence should be addressed. Tel: +81 6 6875 3980; Fax: +81 6 6875 5192; Email: snj-0212@biken.osaka-u.ac.jp

regulatory mechanisms of these events independent of the SC formation event. With this in mind, we have isolated many meiosis-specific genes (20) and found that one of these, *meu13*$^+$, which encodes an ortholog of Hop2, plays an important role in homologous pairing (21). In this paper, we report the identification of an association partner of Meu13, and the functional analysis of this protein. This identification was initially made on the basis that Meu13 harbors a coiled-coil motif that is required for protein–protein interaction (22). We searched the genome database for unidentified *S.pombe* genes that harbor coiled-coil motifs and found one that has a meiosis-specific expression pattern. This gene is referred to as *mcp7*$^+$ (after *m*eiotic *c*oiled-coil *p*rotein) that encodes an ortholog of Mnd1 of *S.cerevisiae* (23), an association partner of Hop2. The *mnd1*-null mutant arrests in meiotic prophase with most DSBs unrepaired and homolog pairing severely reduced (23). Mnd1 is suggested to be involved in strand invasion since *mnd1-1* mutant cells initiated recombination but did not form heteroduplex DNA or Holliday junctions (24). We report here the functional analysis of *mcp7*$^+$.

MATERIALS AND METHODS

Genetics and molecular biology of *S.pombe*

The strains used in this study are listed in Table 1. The media used to promote cell growth and meiosis has been described previously, as have the standard *S.pombe* genetic and molecular biology techniques, including northern analysis, which we employed (25). Surface spreading of chromatin was performed according to Bähler *et al*. (26). Induction of synchronous meiosis and determination of the frequency of meiotic recombination events was assessed as described previously (21,12).

Gene disruption

The *mcp7*$^+$ gene was disrupted by replacing it with the *ura4*$^+$ cassette. To do this, we performed PCR and obtained a DNA fragment carrying the 5′ upstream region and 3′ downstream region of the *mcp7*$^+$ gene. For PCR, we synthesized the following four oligonucleotides and used them as primers: mcp7-5F (5′-CACCGGGGTACCTACTTTATCACCTAAAAATAAAAATGTGTCAACATGTG-3′), mcp7-5R (5′-AGTTCCCTCGAGTGTTTAAAAATTTATTAATTAGTTTGAACAAATATGG-3′), mcp7-3F (5′-TTAAAAACTGCAGACTTGACATGCTTCCTTAATTCAAAGAGTTGTTTTCC-3′), mcp7-3R (5′-CGGGTCGAGCTCGTTTCCAAAGAGAAAGTTCAATATAGCTGTCATAGTTG-3′). The underlined sequences denote the artificially introduced restriction enzyme sites for KpnI, XhoI, PstI and SacI, respectively. These PCR products and the 1.8 kb HindIII fragment containing the *ura4*$^+$ cassette (27) was inserted into the pBluescriptII KS (+) vector via the KpnI–XhoI, PstI–SacI and HindIII sites, respectively. This plasmid construct was digested with KpnI and SacI and the resulting construct was introduced into the haploid strains, TP4-1D and TP4-5A. The Ura$^+$ transformants were then screened by PCR and Southern blot analysis to identify the *mcp7*$^+$*::ura4*$^+$ strain.

Construction of the *mcp7*$^+$*–gfp* strain

To prepare the *mcp7*$^+$*–gfp* construct, we performed PCR and obtained a DNA fragment carrying the open reading frame (ORF) region and the 3′ downstream region of the *mcp7*$^+$ gene. For this purpose, we synthesized the following four oligonucleotides and used them as primers: mcp7ORF-F (5′-AAATAGGCGCGCCGTCGACTATGCCTCCCAAGGGACTATCGCTTGCAGAG-3′), mcp7ORF-R (5′-TTATTCTTAGCGGCCGCCGCAAAATCGGTAGTTGCAGATCGTCCAAATCC-3′). The underlined sequences denote the artificially introduced restriction enzyme sites for AscI–SalI and NotI, respectively. To obtain the 3′ downstream region, we used the same primers as described above. The DNA fragment spanning the ORF of *mcp7*$^+$ was digested by EcoRV and this truncated form of the *mcp7*$^+$ ORF was inserted into *ura4*$^+$-containing pBluescriptII KS (+) vector via EcoRV–NotI. The 3′ downstream region was inserted into the *gfp*-containing pRGT vector via PstI–SacI and cut out by NotI–SacI. Subsequently, the NotI–SacI fragment was inserted into the *ura4*$^+$-containing pBluescriptII KS (+) vector. This plasmid construct was digested with SwaI and the resulting construct was introduced into the haploid strains TP4-5A and TP4-1D. We then screened the Ura$^+$ transformants by PCR, and Southern blot analysis was performed to identify the *mcp7*$^+$*–gfp*-bearing strain. The *mcp7*$^+$*–3ha* strain was also constructed as described above.

Protein extraction

For immunoprecipitation, we followed the protocol where cells were fixed with formaldehyde and destroyed by glass beads without boiling in the Buffer I [50 mM Hepes/KOH (pH 7.5), 140 mM NaCl, 1 mM EDTA (pH 7.5), 1% Triton X-100 (v/v), 0.1% sodiumdeoxycholate (w/v)] (28).

For western analysis, cells ($\sim 2 \times 10^8$) cultured in EMM2-N (+ supplements) were washed by phosphate-buffered saline (PBS), suspended in 0.4 ml HB buffer [25 mM MOPS (pH 7.2), 15 mM $MgCl_2$, 15 mM EGTA, 60 mM β-glycerophosphate, 15 mM *p*-nitrophenylphosphate, 0.1 mM Na_3VO_4, 1 mM DTT], and boiled for 5 min. The cells were then quickly chilled in liquid N_2 and stored at −80°C. Approximately 0.4 ml glass beads was added to pulverize the cells by vigorous vortexing.

Immunoprecipitation of Mcp7–3HA and Meu13–GFP

We added 10 µl protein G-Sepharose beads to 200 µl of the whole cell extract (WCE) and incubated the mixture on a rotating wheel for 1 h at 4°C. The beads were pelleted by centrifugation at 12 000 r.p.m. for 20 s at 4°C and the supernatant was transferred to a fresh 1.5 ml micro-centrifuge tube on ice. This step removes the proteins in the WCE that interact non-specifically with the beads. We then added primary antibodies specific for HA or GFP, namely, rabbit polyclonal anti-HA (MBL Inc., Japan) antibody and rabbit polyclonal anti-GFP antibody (MBL Inc., Japan) at 1 : 50 and 1 : 200 dilutions, respectively to the supernatant and incubated the mixture on a rotating wheel overnight at 4°C. Thereafter, 10 µl of protein G-Sepharose beads were added to the mixture, followed by incubation on a rotating wheel for 1 h at 4°C. We pelleted the beads by centrifugation at 5 000 r.p.m. for 20 s at 4°C, discarded the supernatant, and washed them three times with 1 ml of ice-cold Buffer I. The samples were then subjected to western blot analysis using the rat monoclonal anti-HA antibody 3F10 (Roche) and the rat monoclonal anti-GFP

Table 1. Strains used in this study

Strain name	Genotype
CD16-1[a]	*h*$^+$/*h*$^-$ *ade6-M210/ade6-M216 cyh1/*$^+$ $^+$*/lys5-391*
CD16-5[a]	*h*$^-$/*h*$^-$ *ade6-M210/ade6-M216 cyh1/*$^+$ $^+$*/lys5-391*
TP4-1D	*h*$^+$ *ade6-M216 his2 leu1-32 ura4-D18*
TP4-5A	*h*$^-$ *ade6-M210 leu1-32 ura4-D18*
NP32-2A	*h*$^+$ *his2 leu1-32 ura4-D18*
NP16-6B	*h*$^-$ *ade6-M216 ura4-D18*
ST6-1	*h*$^+$ *ade6-M210 his2 leu1-32 ura4-D18 mcp7::ura4*$^+$
ST6-4	*h*$^-$ *ade6-M216 ura4-D18 mcp7::ura4*$^+$
ST33	*h*$^+$ *ade6-M216 his2 leu1-32 ura4-D18 meu13::ura4*$^+$
ST34	*h*$^-$ *ade6-M210 ura4-D18 meu13::ura4*$^+$
TT102-C	*h*$^+$ *his2 leu1-32 ura4-D18 dmc1::ura4*$^+$
TT103-C	*h*$^-$ *ura4-D18 dmc1::ura4*$^+$
ST106	*h*$^+$ *ade6-M210 his2 leu1-32 ura4-D18 rad17::ura4*$^+$
ST107	*h*$^-$ *ade6-M216 ura4-D18 rad17::ura4*$^+$
ST36	*h*$^+$ *ade6-M210 his2 leu1-32 ura4-D18 mcp7::ura4*$^+$ *meu13::ura4*$^+$
ST35	*h*$^-$ *ade6-M216 ura4-D18 mcp7::ura4*$^+$ *meu13::ura4*$^+$
ST54	*h*$^+$ *ade6-M210 his2 leu1-32 ura4-D18 mcp7::ura4*$^+$ *dmc1::ura4*$^+$
ST55	*h*$^-$ *ade6-M216 ura4-D18 mcp7::ura4*$^+$ *dmc1::ura4*$^+$
ST95	*h*$^+$ *ade6-M210 his2 leu1-32 ura4-D18 mcp7::ura4*$^+$ *rad17::ura4*$^+$
ST96	*h*$^-$ *ade6-M216 ura4-D18 mcp7::ura4*$^+$ *rad17::ura4*$^+$
MS111-W1	*h*$^+$ *ade6-469 his2 leu-32 ura4-D18*
MS105-1B	*h*$^-$ *ade6-M26 ura4-D18*
ST10	*h*$^+$ *ade6-469 his2 leu1-32 ura4-D18 mcp7::ura4*$^+$
ST9	*h*$^-$ *ade6-M26 ura4-D18 mcp7::ura4*$^+$
NP29-5B	*h*$^+$ *ade6-469 his2 leu1-32 ura4-D18 meu13::ura4*$^+$
NP24-1D	*h*$^-$ *ade6-M26 ura4-D18 meu13::ura4*$^+$
TT113	*h*$^+$ *ade6-469 his2 leu1-32 ura4-D18 dmc1::ura4*$^+$
TT112	*h*$^-$ *ade6-M26 ura4-D18 dmc1::ura4*$^+$
MS111-1	*h*$^+$ *ade6-469 his2 leu1-32 ura4-D18 rad17::ura4*$^+$
MS105-22D	*h*$^-$ *ade6-M26 ura4-D18 rad17::ura4*$^+$
ST48	*h*$^+$ *ade6-469 his2 leu1-32 ura4-D18 mcp7::ura4*$^+$ *meu13::ura4*$^+$
ST49	*h*$^-$ *ade6-M26 ura4-D18 mcp7::ura4*$^+$ *meu13::ura4*$^+$
ST56	*h*$^+$ *ade6-469 his2 leu1-32 ura4-D18 mcp7::ura4*$^+$ *dmc1::ura4*$^+$
ST57	*h*$^-$ *ade6-M26 ura4-D18 mcp7::ura4*$^+$ *dmc1::ura4*$^+$
ST97	*h*$^+$ *ade6-469 his2 leu1-32 ura4-D18 mcp7::ura4*$^+$ *rad17::ura4*$^+$
ST99	*h*$^-$ *ade6-M26 ura4-D18 mcp7::ura4*$^+$ *rad17::ura4*$^+$
ST30	*h*$^+$ *ade6-M216 his2 leu1-32 ura4-D18 mcp7::[mcp7*$^+$*–gfp-3′UTR-ura4*$^+$*]*
ST29	*h*$^-$ *ade6-M210 leu1-32 ura4-D18 mcp7::[mcp7*$^+$*–gfp-3′UTR-ura4*$^+$*]*
ST23	*h*$^+$ *ade6-M210 his2 leu1-32 ura4-D18 mcp7::[mcp7*$^+$*–3ha-3′UTR-ura4*$^+$*]*
ST70	*h*$^-$ *ade6-M216 leu1-32 ura4-D18 mcp7::[mcp7*$^+$*–3ha-3′UTR-ura4*$^+$*] pRGT1-meu13*$^+$
JZ670[b]	*h*$^-$/*h*$^-$ *ade6-M210/ade6-M216 leu1-32/leu1-32 pat1-114/pat1-114*
ST31	*h*$^-$/*h*$^-$ *ade6-M216/ade6-M210 leu1-32/leu1-32 ura4-D18/ura4-D18 mcp7::ura4*$^+$*/mcp7::ura4*$^+$ *pat1-114/pat1-114*
KN8	*h*$^-$/*h*$^-$ *ade6-M216/ade6-M210 leu1-32/leu1-32 ura4-D18/ura4-D18 meu13::ura4*$^+$*/meu13::ura4*$^+$ *pat1-114/pat1-114*
MS101-4	*h*$^-$/*h*$^-$ *ade6-M216/ade6-M210 leu1-32/leu1-32 ura4-D18/ura4-D18 rad17::ura4*$^+$*/rad17::ura4*$^+$ *pat1-114/pat1-114*
ST114	*h*$^-$/*h*$^-$ *ade6-M216/ade6-M210 leu1-32/leu1-32 ura4-D18/ura4-D18 rec12::ura4*$^+$*/rec12::ura4*$^+$ *pat1-114/pat1-114*
TK17	*h*$^-$/*h*$^-$ *ade6-M216/ade6-M210 leu1-32/leu1-32 ura4-D18/ura4-D18 mcp7::ura4*$^+$*/mcp7::ura4*$^+$ *meu13::ura4*$^+$*/ meu13::ura4*$^+$ *pat1-114/pat1-114*
ST87	*h*$^-$/*h*$^-$ *ade6-M216/ade6-M210 leu1-32/leu1-32 ura4-D18/ura4-D18 mcp7::ura4*$^+$*/mcp7::ura4*$^+$ *rad17::ura4*$^+$*/ rad17::ura4*$^+$ *pat1-114/pat1-114*
ST88	*h*$^-$/*h*$^-$ *ade6-M216/ade6-M210 leu1-32/leu1-32 ura4-D18/ura4-D18 mcp7::ura4*$^+$*/mcp7::ura4*$^+$ *rec12::ura4*$^+$*/ rec12::ura4*$^+$ *pat1-114/pat1-114*
ST123	*h*$^-$/*h*$^-$ *ade6-M216/ade6-M210 leu1-32/leu1-32 ura4-D18/ura4-D18 mcp7::[mcp7*$^+$*–3ha-3′UTR-ura4*$^+$*]/ mcp7::[mcp7*$^+$*–3ha-3′UTR-ura4*$^+$*] pat1-114/pat1-114*
ST124	*h*$^-$/*h*$^-$ *ade6-M216/ade6-M210 leu1-32/leu1-32 ura4-D18/ura4-D18 mcp7::[mcp7*$^+$*–3ha-3′UTR-ura4*$^+$*]/ mcp7::[mcp7*$^+$*–3ha-3′UTR-ura4*$^+$*] meu13::ura4*$^+$*/meu13::ura4*$^+$ *pat1-114/pat1-114*

Provided by [a]Chikashi Shimoda and [b]Masayuki Yamamoto.

antibody JFP-J5 (Mitsubishi-kagaku Institute of Life Sciences, Tokyo) at 1:1 000 dilutions.

RESULTS

Mcp7 is a meiosis-specific coiled-coil protein that is conserved in a variety of species

To identify a meiosis-specific coiled-coil protein of *S.pombe* that may interact with Meu13, we first searched the genome database for unidentified genes that harbor coiled-coil motifs (http://www.sanger.ac.uk/Projects/S_pombe/), and found 59 genes in this way. We then obtained DNA fragments from each of these genes and used them as probes in northern blot analysis of RNA obtained from *CD16-1* (h^+/h^-) and *CD16-5* (h^-/h^-) cells harvested at various times after the induction of meiosis by nitrogen starvation. This analysis revealed that *mcp7*$^+$ displays meiosis-specific expression that peaks at the horsetail phase (6 h after induction), which is when

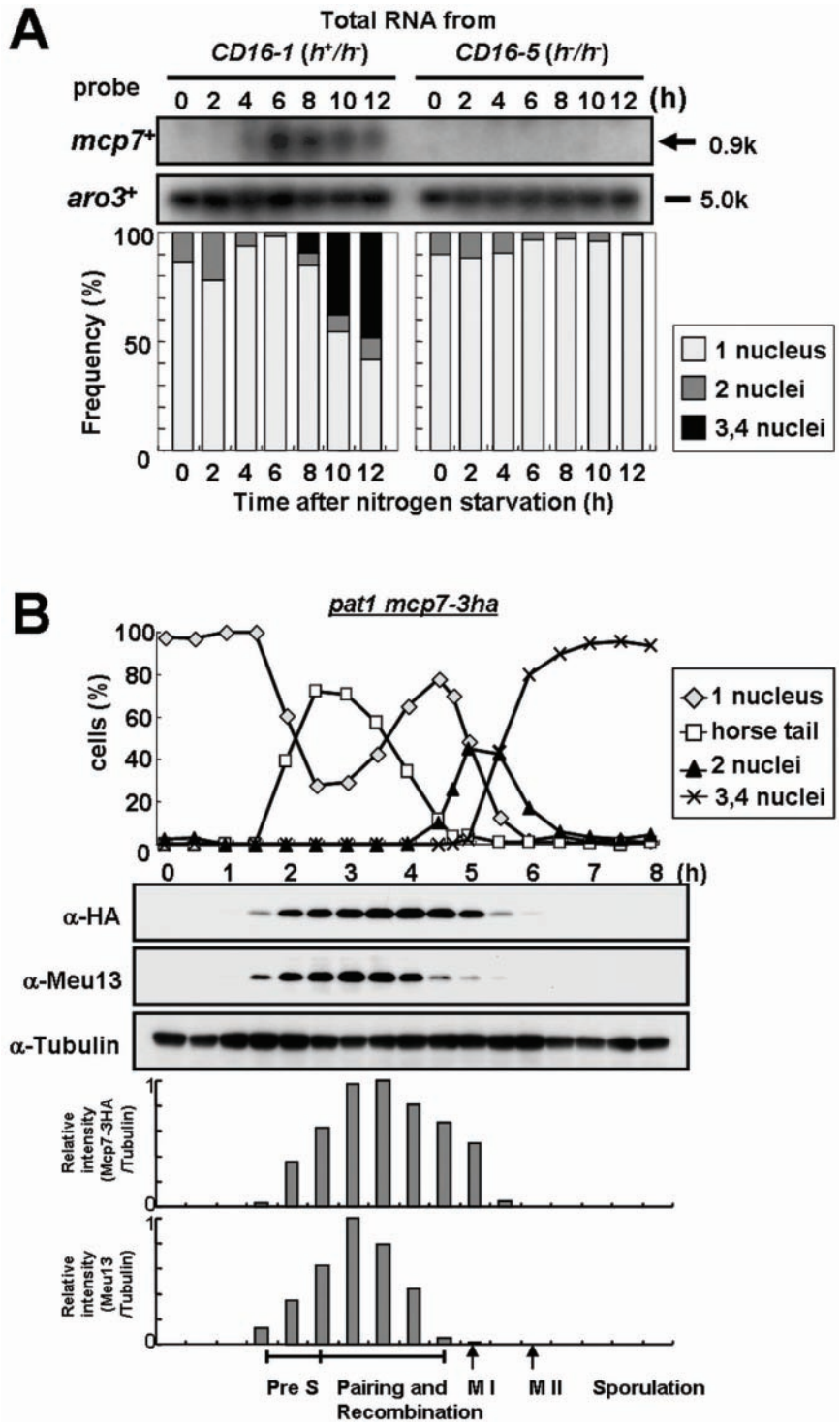

homologous chromosome pairing and recombination occur (Figure 1A).

The production of the Mcp7 protein during meiosis was then assessed by western blot analysis. To attain a synchronized meiotic progression, we replaced *mcp7*$^{+}$ gene of *pat1-114* cell with *mcp7*$^{+}$*–3ha* fusion gene that can express Mcp7 protein tagged with three copies of the HA epitope. Then, the *pat1-114mcp7*$^{+}$*–3ha* diploid cells were induced to enter synchronized meiosis and their lysates were subjected to western blot analysis using an anti-HA antibody. We confirmed that the meiotic progression and spore morphology of *pat1-114mcp7*$^{+}$*–3ha* diploid cells were similar to *pat1-114* cells. As shown in Figure 1B, the timing of appearance of Mcp7–3HA protein during meiosis is the same with that of Meu13, an ortholog of the protein *S.cerevisiae* Hop2, which is required for proper homologous pairing and recombination (15,21). However, the timings of peaks and disappearance of Mcp7 protein are about 30 min delay as compared to those of Meu13.

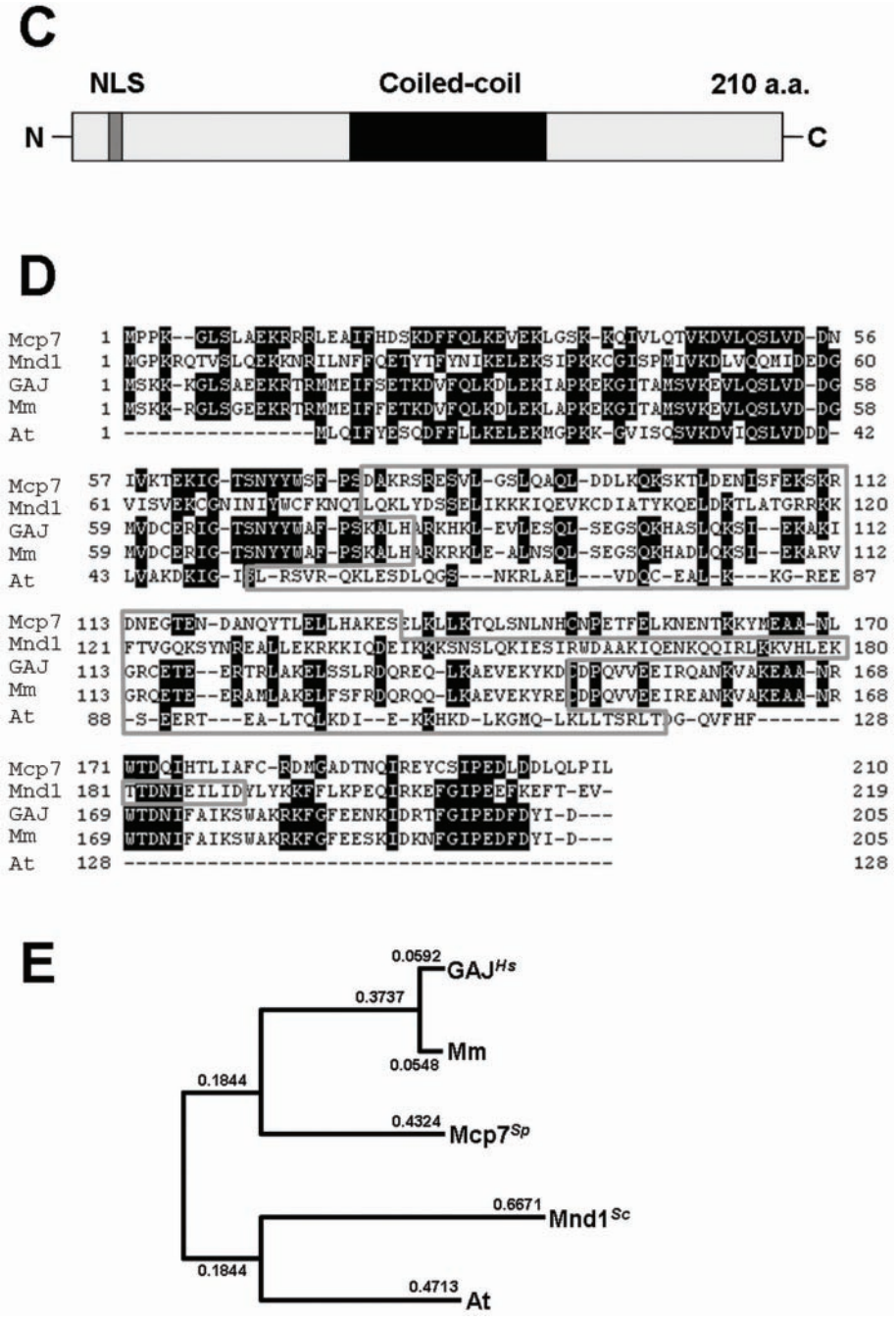

Figure 1. Mcp7 is a meiosis-specific coiled-coil protein that is conserved in a variety of species. (**A**) Northern blot analysis of *mcp7*$^{+}$ and *aro3*$^{+}$ (loading control). Total RNA was extracted from *CD16-1* (h^{+}/h^{-}) and *CD16-5* (h^{-}/h^{-}) cells at the indicated times after meiosis was induced by nitrogen starvation. The RNA was blotted and probed with the ORFs of the *mcp7*$^{+}$ and *aro3*$^{+}$ genes. The graph below indicates the meiotic profiles of the cells used for RNA extraction. Counting at least 200 cells under a microscope assessed the frequencies of Hoechst33342-stained cells that bear one, two, three or four nuclei. (**B**) Western blot analysis of the production of the Mcp7–3HA and Meu13 proteins during the synchronous meiosis of strain ST123. The tubulin levels are also examined as a loading control. To quantify the result, the intensities of the bands were measured by a densitometer and the relative values were presented as bar graphs. (**C**) A schematic presentation of the Mcp7 protein. These motifs were identified by PSORT II (http://psort.nibb.ac.jp/). (**D**) Multiple sequence alignment of Mcp7 with the orthologous proteins in *S.cerevisiae* (Mnd1), *Homo sapiens* (GAJ), *M.musculus* (Mm) and *A.thaliana* (At). Gaps inserted in the alignment to attain maximal homology are indicated by hyphens. The amino acids that are identical between three or more of the five species examined are shaded in black. The gray region indicates a predicted coiled-coil motif. (**E**) The phylogenetic tree of Mcp7. The relationships between the orthologous proteins were inferred by the neighbour-joining method (29). The numbers represent the phylogenetic distance. Both the sequence and phylogenetic analyses were performed by using a GENETYX program (Software Development Co., Ltd).

Mcp7 consists of 210 amino acids and harbors a coiled-coil motif (amino acids 75–134) and a nuclear localization signal (11–14; KRRR) (Figure 1C). Using the BLAST algorithm (http://www.genome.ad.jp/), we identified putative orthologs of Mcp7 in *S.cerevisiae* (Mnd1), *Arabidopsis*, mice and humans (Figure 1D). All of these orthologs bear a coiled-coil motif in the middle. The phylogenetic tree constructed by the neighbor-joining method (29) indicates that the amino

acid sequences of these five Mcp7 orthologs are closely related to one another (Figure 1E). Thus, Mcp7 may play a conserved role in different species.

Mcp7 forms a complex with Meu13 and localizes in the nucleus

Since both Mcp7 and Meu13 harbor a coiled-coil motif, we first investigated by immunoprecipitation analysis whether they form a complex *in vivo*. To do this, lysates of cells expressing Mcp7–3HA and Meu13–GFP were subjected to immunoprecipitation with an anti-GFP antibody followed by western blotting and probing with an anti-HA antibody. This revealed a band of the expected size of Mcp7–3HA (Figure 2A). This suggests that Mcp7 forms a complex with Meu13 *in vivo*. The blot also reveals the presence of another, smaller band that is apparently recognized by the anti-HA antibody. This band did not disappear when the lysates were treated with phosphatase (data not shown), which suggests that it is not a phosphorylated form of Mcp7. Instead, this band disappeared when the cell lysates were boiled just after dissolving them in the HB buffer (see Figure 1B and Materials and Methods). Thus, it may be a degradation product because the cell lysates were kept intact overnight for immunoprecipitation, during which the lysates were exposed to proteases before they were boiled for electrophoresis.

To examine the subcellular localization of Mcp7, we constructed a Mcp7–GFP-expressing strain, induced it to undergo meiosis and observed the GFP signal under a microscope. We considered the Mcp7–GFP fusion protein functional because the *mcp7–gfp* strain showed normal meiotic progression and spore morphology. The Mcp7–GFP protein began to appear in the nucleus at the horsetail period (Figure 2B). This suggests that, like Meu13 (21), Mcp7 localizes in the nucleus during meiosis. To determine whether this nuclear localization is due to the attachment of Mcp7 to the chromosomes, we performed a chromatin spread experiment with *mcp7*$^{+}$*–gfp* cells that were collected 6 h after meiotic induction. The GFP signal was observed on the chromatin in most of the chromatin spreads counted (more than 50), which suggests that Mcp7 is tightly attached to the chromatin (Figure 2C). The result suggests that Mcp7 may be involved in the events on chromatin during meiosis, such as pairing of homologous chromosomes, DNA recombination and/or formation of linear element.

When we confirmed by western blot analysis that Meu13 is expressed in *mcp7*Δ, we found that *mcp7*Δ cells contain less Meu13 protein compared to the *pat1* control strain (Figure 2D-i). This suggests as one of the possibilities that Meu13 is less stable when Mcp7 is absent. On the other hand, as compared to *pat1* control cells, *meu13*Δ cells contain similar amounts of Mcp7–3HA whose expression is prolonged due to the delayed meiosis of *meu13*Δ strain (Figure 2D-ii). The result may also suggest that Mcp7 becomes more stable when Meu13 is absent. This difference in dependence between Mcp7 and Meu13 proteins may explain some of the phenotypic difference between *meu13*Δ and *mcp7*Δ cells (see Discussion).

The mcp7Δ cells are defective in both intergenic and intragenic recombinations

To determine whether, like Meu13 (21), Mcp7 plays a role in meiotic recombination, we measured the rates of intergenic and intragenic recombinations in the *mcp7*Δ strain. For comparison, we also measured them in the *meu13*Δ strain and in a null mutant of a checkpoint *rad*$^{+}$ gene, *rad17*Δ. The *mcp7*Δ*meu13*Δ and *mcp7*Δ*rad17*Δ double null mutants were also assessed.

We first investigated the crossover recombination of zygotic meiosis by tetrad analysis, which allowed us to measure the genetic distance between *leu1* and *his2* (Figure 3A insets). When the *mcp7*Δ strain was crossed, the genetic distance between *leu1* and *his2* was only 5% of the distance obtained when the wild-type strain was crossed. The genetic distances between *leu1* and *his2* that resulted from crossing the *meu13*Δ, *mcp7*Δ*meu13*Δ and *rad17*Δ strains were also largely reduced as compared to wild-type strain (Figure 3A). In the *mcp7*Δ*rad17*Δ strains, spore formation was too poor to analyze statistically (only two four viable spores were detected among 126 tetrads tested).

To further characterize the meiotic recombination competency of the *mcp7*Δ strain, we examined the allelic intragenic recombination between two different mutant alleles of *ade6* (*M26* and *469*). When the *mcp7*Δ strain was crossed, the frequency of its Ade^{+} recombinant spores was 20% of the wild-type frequency (Figure 3B). The frequencies of Ade^{+} recombinant spores obtained by crossing the *meu13*Δ, *mcp7*Δ*meu13*Δ, *rad17*Δ and *mcp7*Δ*rad17*Δ strains constitute 30, 23, 57 and 5%, respectively, of the wild-type frequency. Thus, it appears that Mcp7 plays a significant role in meiotic recombination. It appears that it is as important in this process as Meu13 and even more important than Rad17.

The spores of the *mcp7*Δ strain are abnormal

Next, we observed the spore morphology of *mcp7*Δ cells and found that nearly 20% of the asci displayed abnormal number of ascospores, as some asci include only one, two or three ascospores (Figure 4A). Of the *meu13*Δ asci, 30% also harbored abnormal number of ascospores, and the absence of both genes (the *mcp7*Δ*meu13*Δ double mutant strain) yielded a similar number. However, in the *mcp7*Δ*rad17*Δ double mutant, only 15% of asci showed this abnormality while hardly any abnormalities were observed in the *rad17*Δ asci.

Next, to investigate the DNA distributions in the asci, we stained DNAs with Hoechst33342 and observed them under a microscope. As shown in Figure 4B, ~30% of the asci of the *mcp7*Δ, *meu13*Δ and *mcp7*Δ*meu13*Δ mutants contained abnormal number of nuclei or fragmented DNA, most of them inside and the others outside the ascospores, which indicates that nuclear segregation occurred abnormally in these mutants. However, only 12% of the *rad17*Δ asci showed similar abnormalities, but this value increased up to 62% in the *mcp7*Δ*rad17*Δ double mutant. This is similar to what has been observed for the *meu13*Δ*rad17*Δ double mutant (12). As shown in Figure 4C, the spore viability of *rad17*Δ was similar to that of the wild-type cells, whereas the *mcp7*Δ, *meu13*Δ and *mcp7*Δ*meu13*Δ mutants displayed slightly reduced spore viability. On the other hand, the *mcp7*Δ*rad17* mutant showed significantly reduced spore viability compared with the corresponding single mutants.

These results indicate a close correlation between aberrant spore numbers per ascus (Figure 4A) and percentages of

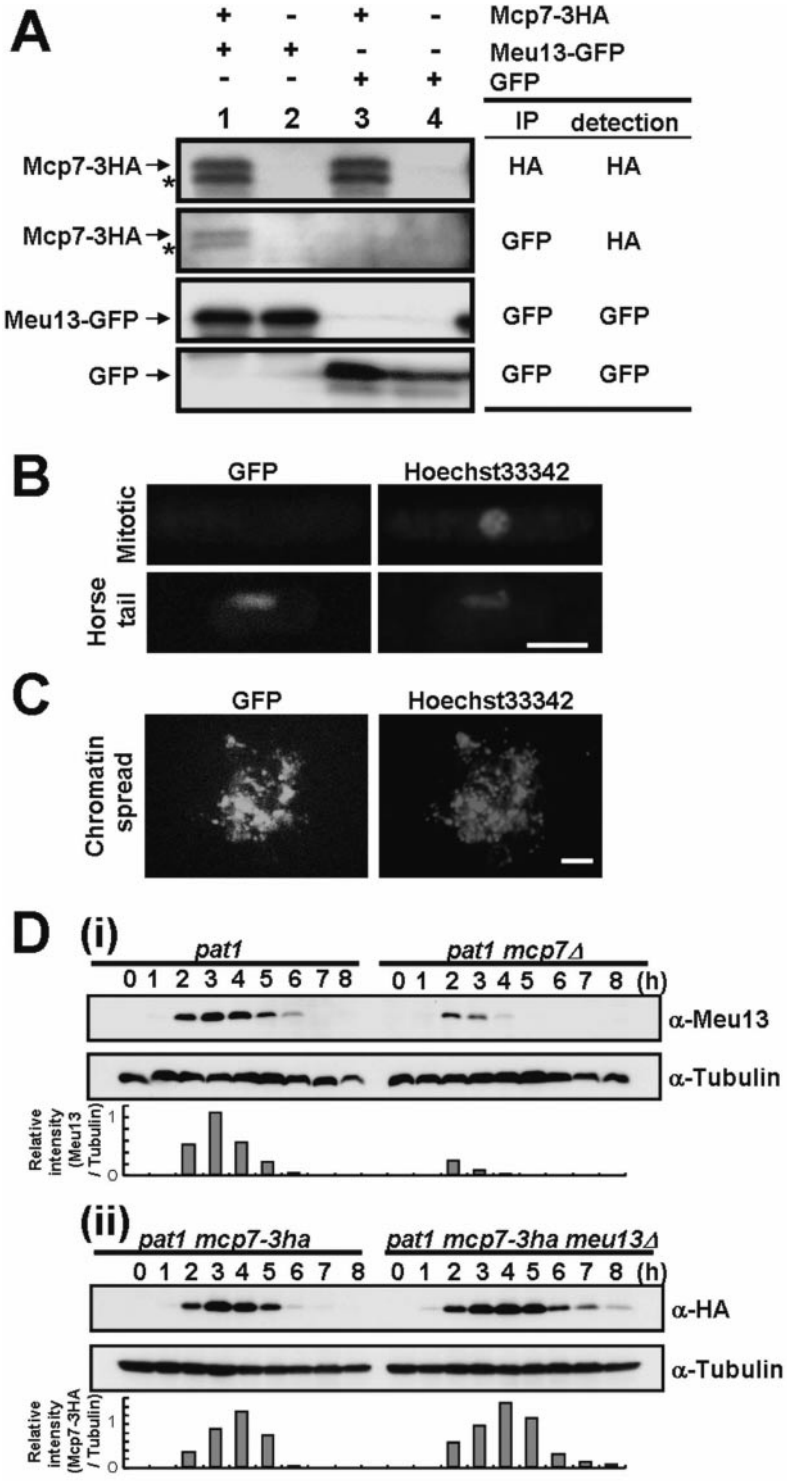

Figure 2. Mcp7 interacts with Meu13 and localizes at meiotic chromatin. (**A**) Immunoprecipitation and western blot analysis of the *in vivo* interaction of Mcp7–3HA and Meu13–GFP. Whole cell extracts prepared from strains expressing Mcp7–3HA and/or Meu13–GFP were subjected to immunoprecipitation with anti-GFP or anti-HA antibodies, after which the immunoprecipitates were subjected to western blot analysis with antibodies bearing the same specificities. Lane 1, Mcp7–3HA and Meu13–GFP; Lane 2, Meu13–GFP; Lane3, Mcp7–3HA and GFP; Lane 4, GFP. The antibodies used in the immunoprecipitation steps are indicated by 'IP', while the antibodies used in the western blot analysis are indicated by 'detection'. Asterisks represent the putative degraded form of Mcp7–3HA. (**B**) Microscopic analysis of Mcp7 localization during meiosis. The *mcp7*$^{+}$*–gfp* strain was induced to enter meiosis by nitrogen starvation and 6 h later the cells were collected for microscopic observation. Bar = 5 μm. (**C**) Chromatin spreads performed using the *mcp7*$^{+}$*–gfp* cells that were collected at 6 h after nitrogen starvation. Bar = 5 μm. (**D**) Western blot analysis of Meu13 levels in the *mcp7*Δ strain and Mcp7 levels in the *meu13*Δ strain. To quantify the result, the intensities of the bands were measured by a densitometer and the relative values were presented as bar graphs. (i) The JZ670 (*pat1-114*) and ST31 (*pat1-114 mcp7*Δ) strains were induced to synchronously enter meiosis and the lysates were subjected to western blot analysis with an anti-Meu13 antibody. Tubulin was detected as a loading control. (ii) The ST123 (*pat1-114 mcp7–3ha*) and ST124 (*pat1-114 mcp7–3ha meu13*Δ) strains were induced to synchronously enter meiosis and the lysates were subjected to western blot analysis with an anti-HA antibody.

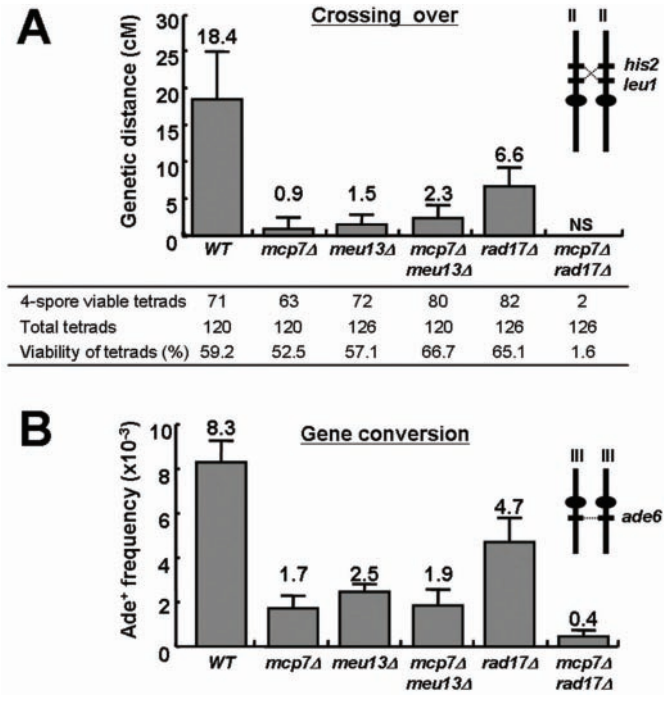

Figure 3. The *mcp7*Δ*rad17*Δ strain shows less recombination than the *mcp7*Δ and *rad17*Δ single mutant strains. (**A**) Crossing over (intergenic recombination). The chromosomal positions of the loci and centromeres are illustrated in the insets. At least 120 tetrads of each strain were analyzed. Only those tetrads that could generate four viable spores were used to calculate genetic distance (cM). The strains examined were *WT* (NP32-2A × NP16-6B), *mcp7*Δ (ST6-1 × ST6-4), *meu13*Δ (ST33 × ST34), *mcp7*Δ*meu13*Δ (ST36 × ST35), *rad17*Δ (ST106 × ST107) and *mcp7*Δ*rad17*Δ (ST95 × ST96). NS, spore formation is too poor to analyze statistically. Data shown are the average values calculated from at least three independent assays. SDs as error bars are indicated. (**B**) Gene conversion (intragenic recombination). The strains used were *WT* (MS111-W1 × MS105-1B), *mcp7*Δ (ST10 × ST9), *meu13*Δ (NP29-5B × NP24-1D), *mcp7*Δ*meu13*Δ (ST48 × ST49), *rad17*Δ (MS111-1 × MS105-22D) and *mcp7*Δ*rad17*Δ (ST97 × ST99). The average values were calculated from at least three independent assays. SDs as error bars are indicated.

unequally segregated nuclei (Figure 4B), except for the *mcp7*Δ*rad17*Δ double mutant where there is good spore formation but many unequally-segregated nuclei. This seems to imply that Rad17 activity delays meiosis to allow some repair of fragmented DNA in *mcp7*Δ/*meu13*Δ backgrounds, but at the cost of defective spore formation. In contrast, spores form mostly normally but DNA is highly fragmented in a *mcp7*Δ*rad17*Δ double mutant, hence yielding the low spore viability (Figure 4C).

*mcp7*Δ cells show a delay in initiation of meiosis I chromosome segregation

We previously showed that *meu13*Δ cells exhibit a delay in initiation of meiosis I chromosome segregation, and that this delay is dependent on *rad17*$^+$, a checkpoint *rad*$^+$ gene (12). To determine whether *mcp7*Δ cells also show similar defects, we monitored their meiotic progression. To synchronize meiosis, we used the *pat1-114* mutant, which enters meiosis in a highly synchronous manner when it is shifted to its restrictive temperature (30). Thus, homozygous diploid *pat1*, *pat1mcp7*Δ, *pat1meu13*Δ and *pat1mcp7*Δ*meu13*Δ cells were arrested at G_1 stage by nitrogen starvation and then shifted to the restrictive temperature (Figure 5A). Meiotic recombination occurs at the horsetail stage, which is when the nucleus moves backwards and forwards several times. The horsetail stage started at similar time points in all the strains tested (~2 h after temperature shift, peaking at ~3 h; data not shown). Thus, the absence of Mcp7 or Meu13 does not appear to affect the entry of *pat1* cells into meiotic prophase.

In the *pat1 meu13*Δ double mutant, appearance of binucleates due to meiosis I chromosome segregation peaked at 5.25 h. This represents a delay as compared to *pat1* peaking at 4.75 h. To show this delay more clearly, number of cells that harbor one, two or more than three nuclei at 4.5 h or 5.25 h after temperature shift to induce meiosis were displayed by bar graphs (Figure 5B). In contrast, the profile of meiotic progression of *pat1mcp7*Δ mutant was similar to *pat1* cells, showing only a slight delay. Notably, the peak (4.75 h) of binucleate appearance of *pat1mcp7*Δ*meu13*Δ cells was almost equal to those of *pat1* cells. This indicates that the meiotic delay of *meu13*Δ mutation was suppressed by additional *mcp7*Δ mutation and that the checkpoint is not triggered in the absence of both Mcp7 and Meu13 (see Discussion). These meiotic progression patterns are reliable because we confirmed them by performing more than three independent experiments and averaging the results.

We further examined the profiles of meiotic progression in *pat1rad17*Δ and *pat1mcp7*Δ *rad17*Δ mutants, and found that they are similar to *pat1* cells (Figure 5B). This suggests that the slight meiotic delay of the *pat1mcp7*Δ cells is partly due to defective recombination or DSB repair, which is monitored by checkpoint *rad*$^+$ proteins such as Rad17 (12). We also investigated the profile of meiotic progression in *rec12*Δ and *mcp7*Δ*rec12*Δ mutants and found that no meiotic delay is observed in these two mutant cells (Figure 5B). The result indicates that the delay in initiation of meiosis I chromosome segregation of *mcp7*Δ cells is Rec12-dependent, namely, it is dependent on meiotic DSB formation. The result suggests that Mcp7 functions after meiotic DSB formation.

Additional *mcp7*Δ mutation in *pat1meu13*Δ cells abolished the delay in phosphorylation of the tyrosine 15 residue of Cdc2

We previously showed that the phosphorylated form of Cdc2 increases during the pre-meiotic S phase of *pat1* cells and then decreases during meiotic division (12). Moreover, we revealed that the delay *pat1meu13*Δ cells show in initiation of meiosis I chromosome segregation is tightly linked to a delay in the dephosphorylation of the tyrosine 15 residue of Cdc2 (12). To determine whether the suppression of meiotic delay by additional *mcp7*Δ mutation in *pat1meu13*Δ cells is linked to Cdc2 dephosphorylation, we performed time-course western blot analysis using an anti-phospho-Cdc2 antibody. As shown in Figure 6, the timing of tyrosine 15 dephosphorylation of Cdc2 in the *pat1mcp7*Δ*meu13*Δ triple mutant cells was almost similar to the *pat1* control. The delay in tyrosine 15 dephosphorylations of the *pat1meu13*Δ cells was pronounced as we reported previously (12), whereas only a slight delay is observed in *pat1mcp7*Δ cells. The results are consistent

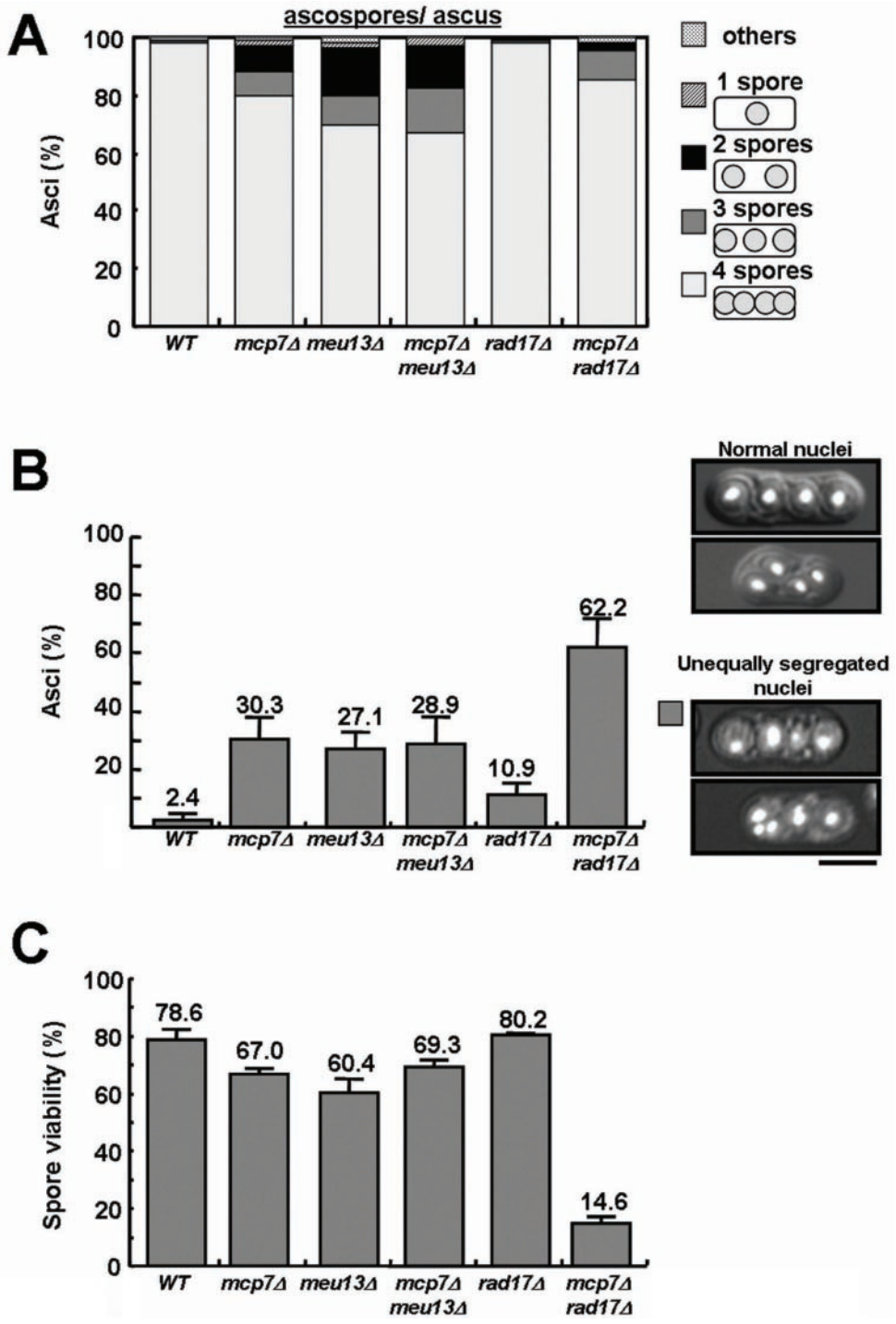

Figure 4. The spores of the *mcp7*Δ strain are abnormal. (**A**) Number of ascospores per ascus in the *mcp7*Δ, *meu13*Δ and *rad17*Δ single and double mutants. The diploid strains were induced to enter meiosis by nitrogen starvation, harvested 18 h later and fixed with 70% ethanol for staining with Hoechst33342. At least 200 cells were counted for a mutant. (**B**) Frequency of abnormal ascospores carrying unequally segregated nuclei in the *mcp7*Δ, *meu13*Δ and *rad17*Δ single and double mutants. Data shown are the average values calculated from at least three independent counting. At least 200 cells were counted for a mutant. (**C**) Spore viability of the *mcp7*Δ, *meu13*Δ and *rad17*Δ single and double mutants. Random spore analysis was performed. Data shown are the average values calculated from at least three independent assays (84 spores were counted per assay). SDs as error bars are indicated.

with the onset timing of meiosis I chromosome segregation in these mutant cells (Figure 5A and B). These results indicate that the suppression of meiotic delay in *pat1meu13*Δ cells by additional *mcp7*Δ mutation is also tightly linked to the tyrosine 15 dephosphorylation of Cdc2.

Mcp7 and Dmc1 act in the same pathway

We previously reported that disruption of Dmc1 function caused meiotic delay (12). To know if *mcp7*$^{+}$ shows any genetic interactions with *dmc1*$^{+}$, we first compared the

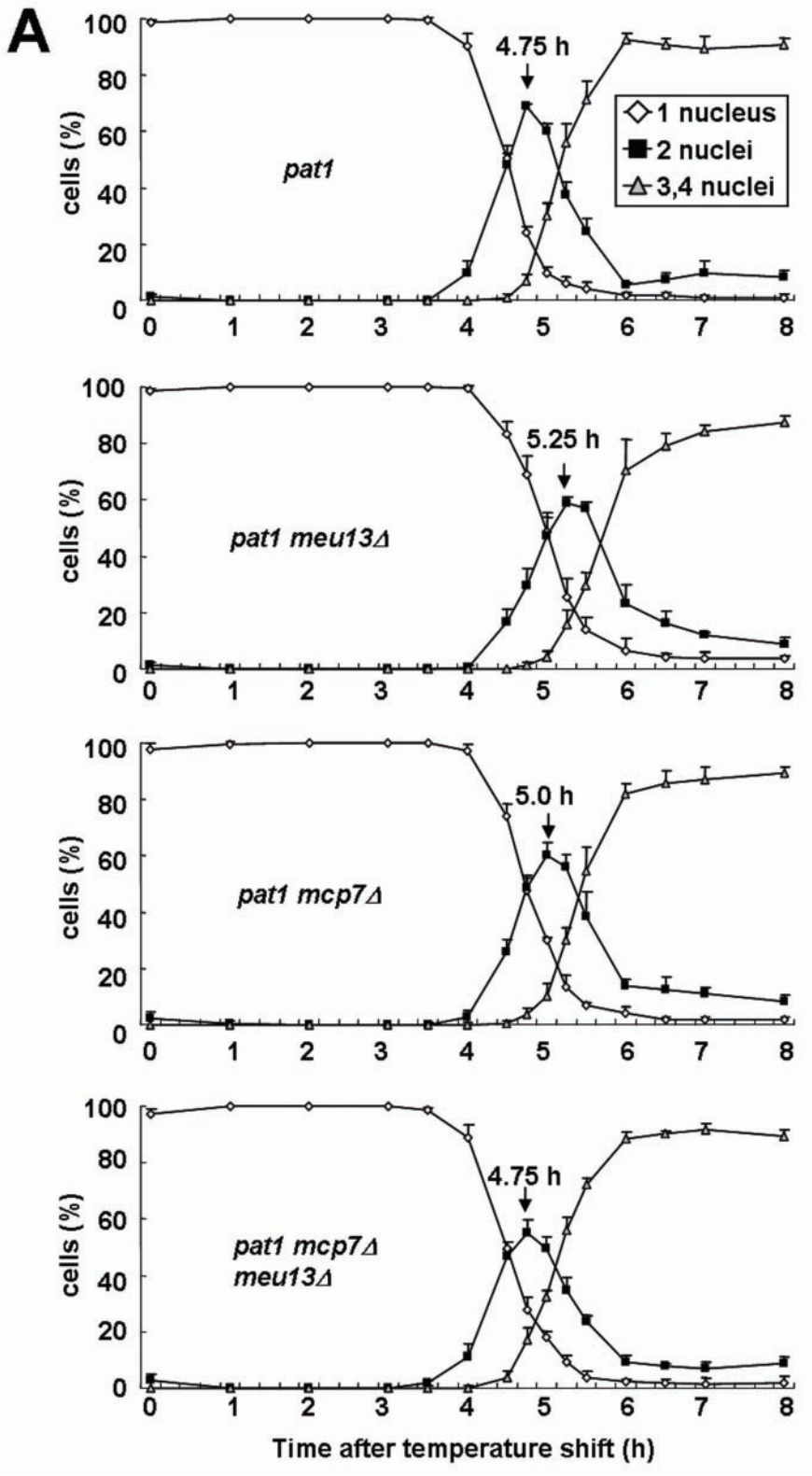

recombination rates between *mcp7*Δ and *dmc1*Δ mutants. As shown in Figure 7A, the rates of crossing over were severely reduced in *mcp7*Δ, and *dmc1*Δ cells. Gene conversion rates were also reduced similarly in these mutant cells (Figure 7B). The *mcp7*Δ*dmc1*Δ double mutant shows similar levels of crossing over and gene conversion rates to *dmc1*Δ mutant. These results suggest that Mcp7 and Dmc1 play key roles in meiotic recombination in the same pathway. Similarly in

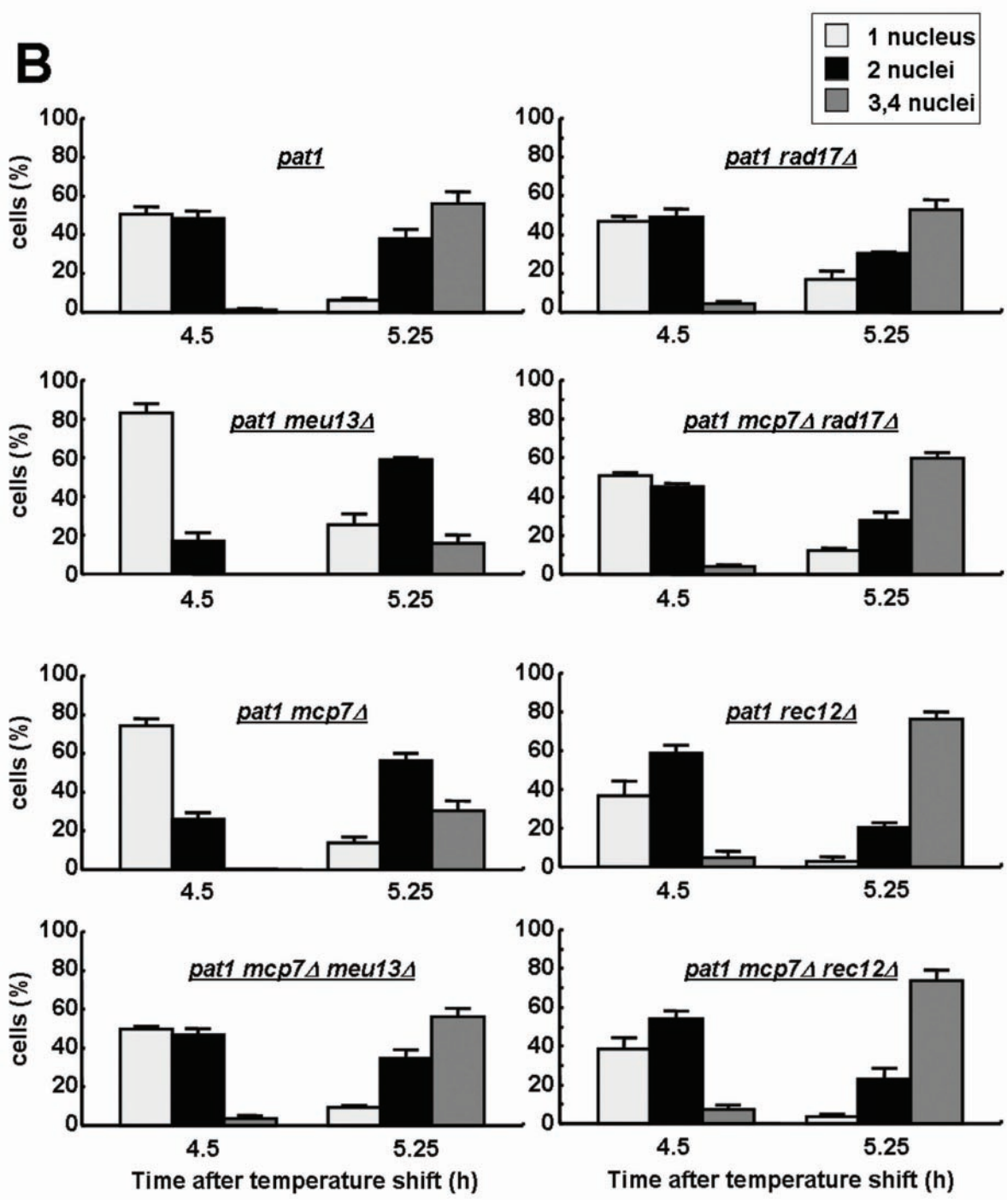

Figure 5. The *mcp7*Δ strain shows a *rad17*$^{+}$-dependent delay in initiation of meiosis I chromosome segregation. (**A**) Meiotic progression of the *mcp7*Δ and *meu13*Δ single and double mutants. Fresh homozygous *pat1-114* diploid strains were cultured in EMM2 medium at 25°C until mid-log phase, transferred to EMM2-N medium for 16 h at 25°C, and then shifted to 34°C to inactivate Pat1 and synchronize meiosis. The progression of meiosis was monitored every 15 min, 30 min or 1 h after the temperature shift depending on the phase of meiosis. Each point denotes the average value of at least three independent experiments. (**B**) Average ratios of the *pat1mcp7*Δ, *pat1meu13*Δ, *pat1mcp7*Δ*meu13*Δ, *pat1 rad17*Δ and *pat1mcp7*Δ*rad17*Δ, *pat rec12*Δ, *pat1mcp7*Δ*rec12*Δ cells that carry 1 nucleus, 2 nuclei and more than 3 nuclei as observed by Hoechst33342 at 4.5 and 5.25 h. In all experiments, at least 200 cells at every points of each time course of meiotic progression were counted under a microscope, and at least three independent experiments were conducted to examine the time-course for each strain. Average values of three independent measurements and SDs as error bars are indicated.

S.cerevisiae, Mnd1 is supposed to operate downstream of Dmc1 binding to DNA (24).

The spore viability of *mcp7*Δ mutant was slightly lowered as compared to wild-type and *dmc1*Δ mutants (Figure 7C). On the other hand, the spore viability of *mcp7*Δ*dmc1*Δ double mutant was a wild-type level. We also observed DNAs in the asci by staining them with Hoechst33342 and found that the percentages of the asci harboring unequally distributed DNA contents

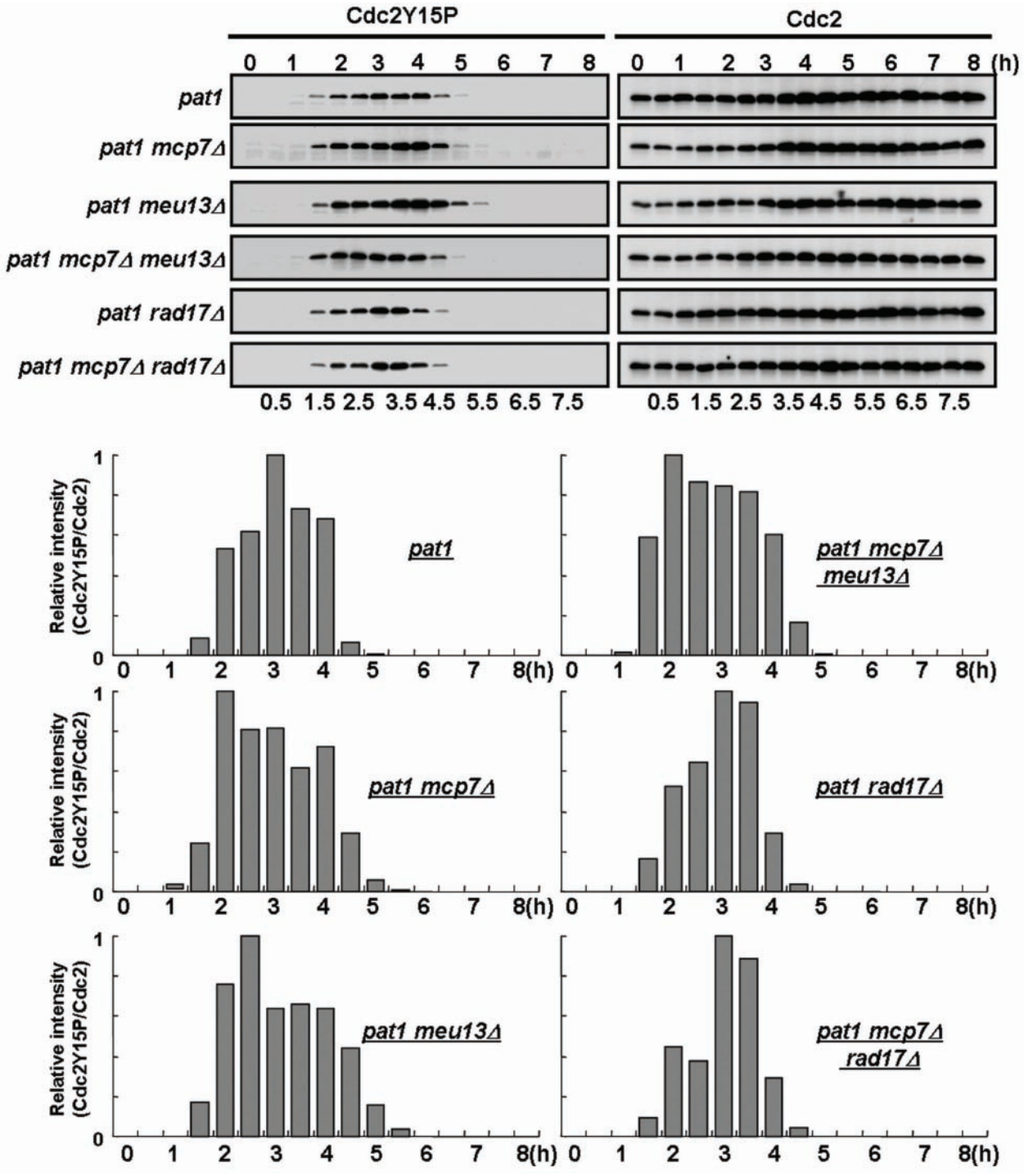

Figure 6. The dephosphorylation of the Tyr15 residue of Cdc2 is slightly prolonged in *pat1mcp7*Δ cells compared to *pat1* cells. *pat1* (JZ670), *pat1mcp7*Δ (ST31), *pat1meu13*Δ (KN8), *pat1mcp7*Δ*meu13*Δ (TK17), *pat1rad17*Δ (MS101-4) and *pat1mcp7*Δ*rad17*Δ (ST87) cells were induced to enter meiosis as described in the legend to Figure 5. Samples were taken after the temperature shift at the indicated time points and western blot analysis was performed to detect the Cdc2 and phosphorylated Cdc2 levels. To quantify the result, the intensities of the bands were measured by a densitometer and the relative values were presented as bar graphs.

increased to 30.3 and 15.5% in *mcp7*Δ and *dmc1*Δ cells, respectively (Figure 7D). Notably, the percentage of *mcp7*Δ*dmc1*Δ double mutant (16.6%) was similar to that of *dmc1*Δ mutant, suggesting that absence of Mcp7 in *dmc1*Δ cells had no effect on failure in DSB repair that caused aberrant separation of chromosomes. These results indicate that Mcp7 acts in the downstream of Dmc1 for recombination, chromosome separation and subsequent sporulation. Similarly, *dmc1* is reported to be epistatic to *hop2* for sporulation in *S.cerevisiae* (16).

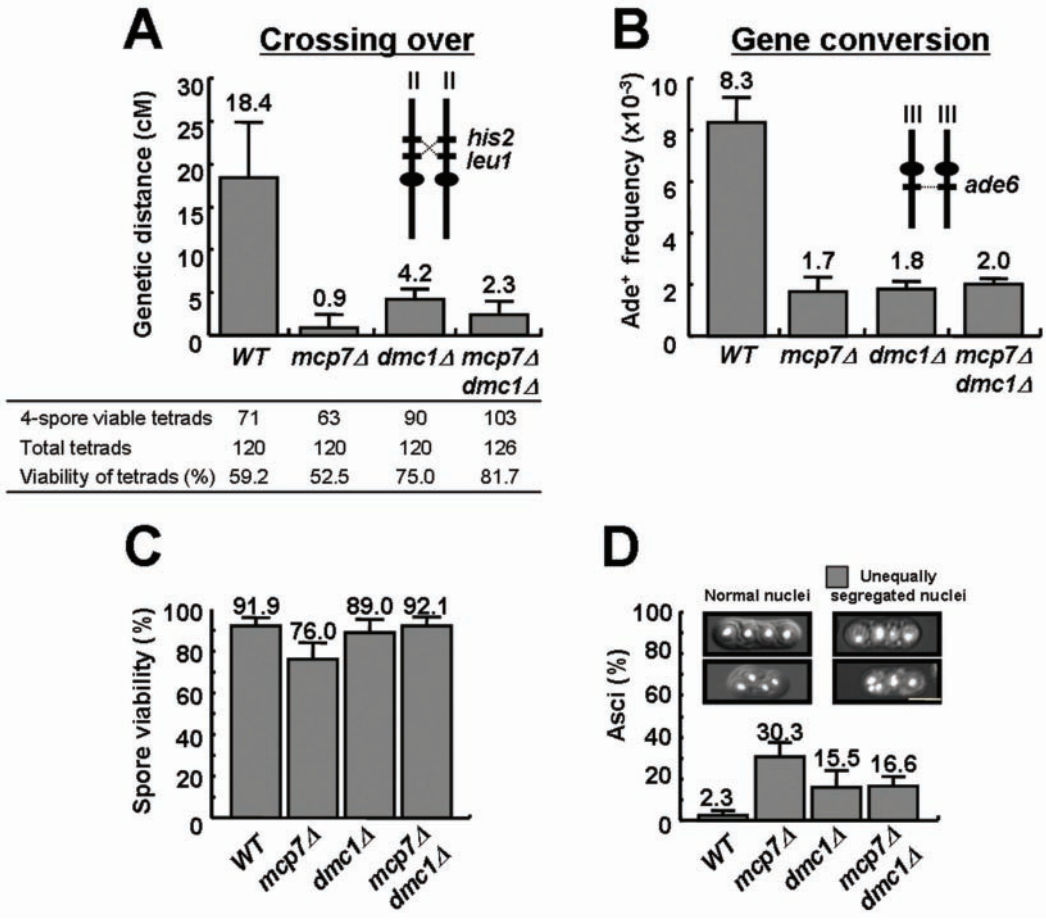

4-spore viable tetrads	71	63	90	103
Total tetrads	120	120	120	126
Viability of tetrads (%)	59.2	52.5	75.0	81.7

Figure 7. Mcp7 genetically interacts with Dmc1 in recombination and spore formation. (**A**) Frequency of crossing over in the wild-type, *mcp7*Δ, *dmc1*Δ and *mcp7*Δ*dmc1*Δ cells. The chromosomal positions of the loci and centromeres are illustrated in the insets. The average values were calculated from at least three independent assays with SDs as error bars (at least 40 tetrads were dissected per assay). The mutant strains examined were *mcp7*Δ (ST6-1 × ST6-4), *dmc1*Δ (TT102-C × TT103-C) and *mcp7*Δ*dmc1*Δ (ST54 × ST55). (**B**) Frequency of gene conversion. The average values were calculated from at least three independent assays denoting SDs as error bars. (**C**) Spore viability. Tetrads were dissected by micromanipulator. Data shown are the average values calculated from at least three independent assays (at least 21 tetrads were dissected per assay). SDs as error bars are indicated. (**D**) Frequency of abnormal ascospores carrying unequally segregated nuclei. The diploid strains were induced to enter meiosis by nitrogen starvation, harvested 18 h later and fixed with 70% ethanol for staining with Hoechst33342. Data shown are the average values calculated from at least three independent counting. At least 200 cells were counted for a mutant.

DISCUSSION

Mcp7 and Meu13 show similar properties and cooperate during meiosis

In the present study, we show that Mcp7 associates with Meu13 to play a role in meiotic recombination and generation of normal spores, probably due to appropriate chromosome pairing. We demonstrate here that these two proteins share the following similar properties. First, their sizes are similar (210 and 216 amino acids), and they both harbor a centrally located coiled-coil motif. Second, they are both evolutionarily conserved among species as their orthologs are found in humans, mice, plants and budding yeast, although the nematode and the fly are exceptions to this, as is discussed above. Third, they are specifically expressed during meiosis at similar time points, namely, at the pre-S phase through to meiosis II, peaking at the horsetail phase (Figure 1A). Fourth, they both localize to the nucleus, in particular, on chromatin (Figure 2B and 2C). Fifth, the phenotypes of the null mutants are similar, showing reduced recombination rates and spore viability (Figures 3 and 4C). They also produce spores with abnormal morphology (Figure 4). Sixth, some of these properties are dependent on *rad17*$^+$, a checkpoint *rad*$^+$ gene.

Like Mnd1 and Hop2 of *S.cerevisiae* (23), we assume that Mcp7 and Meu13 cooperate during meiosis through interaction with each other. Evidence supporting this is that when they are both expressed within a cell, antibodies specific for one co-immunoprecipitate the other (Figure 2A). This suggests that these proteins can form a complex *in vivo*. The result indicates that Mcp7 and Meu13 form a complex during meiosis and as components of the Meu13 protein complex, they may cooperatively participate in homologous chromosome pairing (21).

Mcp7 and Meu13 distinctly cooperate during meiosis

On the other hand, Mcp7 and Meu13 differ in the following properties. First, Mcp7 and Meu13 show no homology in their amino acid sequences, and Mcp7 alone harbors a nuclear localization signal. Second, their meiotic progression patterns

differ slightly, namely, the delay in initiation of meiosis I chromosome segregation is less apparent in *mcp7*Δ cells than in *meu13*Δ cells (Figure 5A). Third, the timing of disappearance during meiosis of Mcp7 protein is 30 min after that of Meu13 (Figure 1B). Fourth, Mcp7 protein is stable in *meu13*Δ cells, whereas Meu13 protein is unstable in *mcp7*Δ cells during meiosis (Figure 2D).

It is notable that *mcp7*Δ*meu13*Δ double mutants exhibit no delay, not only in initiation of meiosis I chromosome segregation but also in dephosphorylating the tyrosine 15 residue of Cdc2. This phenotype can be explained as follows although it is speculative with the present results: delays in meiotic progressions in *mcp7*Δ and *meu13*Δ cells are due to the meiotic checkpoint that may monitor aberrant pairing between non-homologous chromosomes (12,15,21,23). Mcp7 and Meu13 cooperate to form proper pairing between homologous chromosomes in wild-type cells. However, in the absence of association partners in *mcp7*Δ or *meu13*Δ cells, Meu13 proteins alone or Mcp7 proteins alone are considered to promote aberrant chromosome pairing in proportion to their amounts. Since the amount of Meu13 proteins in *mcp7*Δ cells is much less than that of Mcp7 proteins in *meu13*Δ cells (Figure 2D), a larger amount of aberrantly paired chromosome is expected to exist in *meu13*Δ cells than *mcp7*Δ cells. These aberrantly paired chromosomes may trigger the meiotic checkpoint machinery to delay meiotic progression before they are repaired. The extent of meiotic delay may be in proportion to the aberrantly paired chromosome to be repaired, which explains why the delay of *meu13*Δ cells is larger than *mcp7*Δ cells (Figure 5). The amount of aberrantly paired chromosomes, however, may be reduced because of inefficient chromosome pairing itself in the absence of both Mcp7 and Meu13 proteins, and thus no triggering of checkpoint may occur in *mcp7*Δ*meu13*Δ double mutant cells, explaining the absence of meiotic delay. Examination of these assumptions in *S.pombe* will require further technical developments.

Evolutionary conservation of Mcp7/Meu13 function

Mcp7 is an ortholog of the Mnd1 protein of *S.cerevisiae* (23,24). Mcp7 is similar to Mnd1 in that both proteins are meiosis-specific chromosomal proteins that harbor a coiled-coil motif and that are required for meiotic recombination. Moreover, they need at least one association partner to fulfill their functions, namely, Mcp7 interacts with Meu13 while Mnd1 interacts with Hop2 (15).

Orthologs of Mcp7 and Meu13 have been identified in *S.cerevisiae*, *Arabidopsis*, mice and humans as described above. Mnd1 and Hop2 depend on each other for their nuclear localization and it has been reported that they also form a stable complex (23). In *S.cerevisiae*, when SC formation is abnormal due to the defect in homologous chromosome pairing or recombination, meiosis arrests at the pachytene stage (23). In contrast, in *S.pombe*, meiosis is not arrested even in such abnormal cases. However, recombination-defective mutants of *S.pombe*, such as the *meu13*Δ strain, will delay their initiations of meiosis I chromosome segregation, and this delay is imposed by the monitoring system that is called the 'meiotic recombination checkpoint' (12). Notably, orthologs of Mcp7 and Meu13 have not been identified in *C.elegans* and *D.melanogaster*. SC formation also differs in these organisms in that Spo11 is not required for synapsis in *C.elegans* (31) and *D.melanogaster* (32) but is required for synapsis in *S.cerevisiae* (33), mice (9,10) and *Arabidopsis* (8). Thus, the mechanism regulating synapsis in *C.elegans* and *D.melanogaster* may have evolved differently. It may be that orthologs of Mcp7 and Meu13 are required only in organisms that have selected homologous recombination as an essential event in chromosome synapsis.

Our result suggests that Mcp7 forms a complex with Meu13 that plays a key role in chromosome pairing (21) and seems to act after the formation of meiotic DSBs (Figure 5D). In *S.cerevisiae*, Hop2/Mnd1 complex promotes meiotic chromosome pairing and DSB repair (23). We also showed that Mcp7 functions in the downstream of Dmc1 (Figure 7). Similarly, Mnd1 operates downstream of Dmc1 binding to DNA (24), and Hop2 functions in the downstream of Dmc1 for sporulation (16). Thus, function of Mcp7/Meu13 complex seems to be conserved among these species.

ACKNOWLEDGEMENTS

We would like to thank Prof. Chikashi Shimoda and Prof. Masayuki Yamamoto for *S.pombe* strains. We thank Ms Tomoko Motoyama for technical assistance, and Dr Patrick Hughes for critical reading of the manuscript. This work was supported by a Grant-in-aid for Scientific Research on Priority Areas from the Ministry of Education, Science, Sports and Culture of Japan and grants from The Uehara Foundation.

REFERENCES

1. Zickler,D. and Kleckner,N. (1999) Meiotic chromosomes: integrating structure and function. *Annu. Rev. Genet.*, **33**, 603–754.
2. Burgess,S.M. (2002) Homologous chromosome associations and nuclear order in meiotic and mitotically dividing cells of budding yeast. *Adv. Genet.*, **46**, 49–90.
3. Page,S.L. and Hawley,R.S. (2003) Chromosome choreography: the meiotic ballet. *Science*, **301**, 785–789.
4. Martini,E and Keeney,S. (2002) Sex and the single (double-strand) break. *Mol. Cell*, **9**, 700–702.
5. Cervantes,M.D., Farah,J.A. and Smith,G.R. (2000) Meiotic DNA breaks associated with recombination in *S.pombe*. *Mol. Cell*, **5**, 883–888.
6. Davis,L. and Smith,G.R. (2001) Meiotic recombination and chromosome segregation in *Schizosaccharomyces pombe*. *Proc. Natl Acad. Sci. USA*, **98**, 8395–8402.
7. Davis,L. and Smith,G.R. (2003) Nonrandom homolog segregation at meiosis I in *Schizosaccharomyces pombe* mutants lacking recombination. *Genetics*, **163**, 857–874.
8. Grelon,M., Vezon,D., Gendrot,G. and Pelletier,G. (2001) AtSPO11-1 is necessary for efficient meiotic recombination in plants. *EMBO J.*, **20**, 589–600.
9. Baudat,F., Manova,K., Yuen,J.P., Jasin,M. and Keeney,S. (2000) Chromosome synapsis defects and sexually dimorphic meiotic progression in mice lacking Spo11. *Mol. Cell*, **6**, 989–998.
10. Romanienko,P.J. and Camerini-Otero,R.D. (2000) The mouse Spo11 gene is required for meiotic chromosome synapsis. *Mol. Cell*, **5**, 975–987.
11. Bailis,J.M. and Roeder,G.S. (2000) The pachytene checkpoint. *Trends Genet.*, **16**, 395–403.
12. Shimada,M., Nabeshima,K., Tougan,T. and Nojima,H. (2002) The meiotic recombination checkpoint is regulated by checkpoint *rad*$^{+}$ genes in fission yeast. *EMBO J.*, **21**, 2807–2818.
13. Hong,E.J. and Roeder,G.S. (2002) A role for Ddc1 in signaling meiotic double-strand breaks at the pachytene checkpoint. *Genes Dev.*, **16**, 363–376.

14. Tarsounas,M. and Moens,P.B. (2001) Checkpoint and DNA-repair proteins are associated with the cores of mammalian meiotic chromosomes. *Curr. Top. Dev. Biol.*, **51**, 109–134.
15. Leu,J.Y., Chua,P.R. and Roeder,G.S. (1998) The meiosis-specific Hop2 protein of *S.cerevisiae* ensures synapsis between homologous chromosomes. *Cell*, **94**, 375–386.
16. Tsubouchi,H. and Roeder,G.S. (2003) The importance of genetic recombination for fidelity of chromosome pairing in meiosis. *Dev. Cell*, **5**, 915–925.
17. Petukhova,G.V., Romanienko,P.J. and Camerini-Otero,R.D. (2003) The Hop2 protein has a direct role in promoting interhomolog interactions during mouse meiosis. *Dev. Cell*, **5**, 927–936.
18. MacQueen,A.J., Colaiacovo,M.P., McDonald,K. and Villeneuve,A.M. (2002) Synapsis-dependent and -independent mechanisms stabilize homolog pairing during meiotic prophase in *C. elegans*. *Genes Dev.*, **16**, 2428–2442.
19. Liu,H., Jang,J.K., Kato,N. and McKim,K.S. (2002) mei-P22 encodes a chromosome-associated protein required for the initiation of meiotic recombination in *Drosophila melanogaster*. *Genetics*, **162**, 245–258.
20. Watanabe,T., Miyashita,K., Saito,T.T., Yoneki,T., Kakihara,Y., Nabeshima,K., Kishi,Y.A., Shimoda,C. and Nojima,H. (2001) Comprehensive isolation of meiosis-specific genes identifies novel proteins and unusual non-coding transcripts in *Schizosaccharomyces pombe*. *Nucleic Acids Res.*, **29**, 2327–2337.
21. Nabeshima,K., Kakihara,Y., Hiraoka,Y. and Nojima,H. (2001) A novel meiosis-specific protein of fission yeast, Meu13p, promotes homologous pairing independently of homologous recombination. *EMBO J.*, **20**, 3871–3881.
22. Burkhard,P., Stetefeld,J. and Strelkov,S.V. (2001) Coiled coils: a highly versatile protein folding motif. *Trends Cell Biol.*, **11**, 82–88.
23. Tsubouchi,H. and Roeder,G.S. (2002) The Mnd1 protein forms a complex with Hop2 to promote homologous chromosome pairing and meiotic double-strand break repair. *Mol. Cell. Biol.*, **22**, 3078–3088.
24. Gerton,J.L. and DeRisi,J.L. (2002) Mnd1p: an evolutionarily conserved protein required for meiotic recombination. *Proc. Natl Acad. Sci. USA*, **99**, 6895–6900.
25. Okuzaki,D., Satake,W., Hirata,A. and Nojima,H. (2003) Fission Yeast *meu14*$^{+}$ is required for proper nuclear division and accurate formation of forespore membrane during meiosis II. *J. Cell. Sci.*, **116**, 2721–2731.
26. Bähler,J., Wyler,T., Loidl,J. and Kohli,J. (1993) Unusual nuclear structures in meiotic prophase of fission yeast: a cytological analysis. *J. Cell Biol.*, **121**, 241–256.
27. Grimm,C., Kohli,J., Murray,J. and Maundrell,K. (1988) Genetic engineering of *Schizosaccharomyces pombe*: a system for gene disruption and replacement using the *ura4*$^{+}$ gene as a selectable marker. *Mol. Gen. Genet.*, **215**, 81–86.
28. Takahashi,K., Saitoh,S. and Yanagida,M. (2000) Application of the chromatin immunoprecipitation method to identify *in vivo* protein–DNA associations in fission yeast. *Sci. STKE*, **56**, 1–10.
29. Saitou,N. and Nei,M. (1987) The neighbour-joining method: a new method for reconstructing phylogenetic trees. *Mol. Biol. Evol.*, **4**, 406–425.
30. Iino,Y. and Yamamoto,M. (1985) Mutants of *Schizosaccharomyces pombe* which sporulate in the haploid state. *Mol. Gen. Genet.*, **198**, 416–421.
31. Dernburg,A.F., McDonald,K., Moulder,G., Barstead,R., Dresser,M. and Villeneuve,A.M. (1998) Meiotic recombination in *C. elegans* initiates by a conserved mechanism and is dispensable for homologous chromosome synapsis. *Cell*, **94**, 387–398.
32. McKim,K.S., Green-Marroquin,B.L., Sekelsky,J.J., Chin,G., Steinberg,C., Khodosh,R. and Hawley,R.S. (1998) Meiotic synapsis in the absence of recombination. *Science*, **279**, 876–878.
33. Cha,R.S., Weiner,B.M., Keeney,S., Dekker,J. and Kleckner,N. (2000) Progression of meiotic DNA replication is modulated by interchromosomal interaction proteins, negatively by Spo11p and positively by Rec8p. *Genes Dev.*, **14**, 493–503.